The Canadian Mineralogist
Vol. 34, pp. 1089-1105 (1996)

STATIC AND DYNAMIC JAHN–TELLER EFFECTS IN Cu^{2+} OXYSALT MINERALS

PETER C. BURNS[1] AND FRANK C. HAWTHORNE

Department of Geological Sciences, University of Manitoba, Winnipeg, Manitoba R3T 2N2

ABSTRACT

The details of Jahn–Teller distorted $Cu^{2+}\phi_6$ (ϕ: O^{2-}, OH^-, H_2O) octahedral geometries in Cu^{2+} oxysalt minerals are examined. Usually the $Cu^{2+}\phi_6$ octahedron is (4 + 2)-distorted, although both (2 + 4)-distorted and holosymmetric octahedra have been reported in mineral structures. To a first order, the Jahn–Teller theorem indicates that either a (4 + 2) or (2 + 4) distortion of the $Cu^{2+}\phi_6$ octahedron is equally likely to occur, in apparent conflict with the dominance of (4 + 2)-distorted octahedra; this requires an extension of the Jahn–Teller theorem. Examination of reported holosymmetric $Cu^{2+}\phi_6$ octahedra in mineral structures shows that there is no conclusive evidence of a holosymmetric $Cu^{2+}\phi_6$ octahedron. The presence of (2 + 4)-distorted $Cu^{2+}\phi_6$ octahedra in the structures of volborthite and $KCu_3^{2+}(OH)_2[(AsO_4)H(AsO_4)]$, and a (2 + 2 + 2)-distorted $Cu^{2+}\phi_6$ octahedron in the structures of bayldonite and cyanochroite is attributed to a dynamic Jahn–Teller effect, rather than the static distortion that is usual in $Cu^{2+}\phi_6$ oxysalt structures. The most persuasive example of a true (2 + 4)-distorted $Cu^{2+}\phi_6$ octahedron occurs in the structure of demesmaekerite.

Keywords: Cu^{2+} oxysalt minerals, Jahn–Teller effect, structural distortion, dynamic distortion.

SOMMAIRE

Les détails de la géométrie des octaèdres $Cu^{2+}\phi_6$ (ϕ: O^{2-}, OH^-, H_2O) rendus difformes à cause de l'effet de Jahn et Teller dans les oxysels de Cu^{2+} font l'objet de ce travail. En général, les octaèdres $Cu^{2+}\phi_6$ sont difformes selon le schéma (4 + 2), quoique les octaèdres difformes (2 + 4) et les octaèdres holosymétriques ont aussi été découverts dans les structures de minéraux. Comme première approximation, le théorème de Jahn et Teller prédit que la distorsion d'un octaèdre $Cu^{2+}\phi_6$ pourrait être soit (4 + 2) ou (2 + 4), avec chances égales de développement. Cette prédiction ne semble pas conforme aux observations empiriques d'une dominance d'octaèdres difformes (4 + 2), et impose donc une extension du théorème. Un examen des cas d'octaèdres holosymétriques $Cu^{2+}\phi_6$ dans les structures de minéraux décrites dans la littérature montre que l'évidence n'est pas concluante pour l'existence de ceux-ci. La présence d'octaèdres $Cu^{2+}\phi_6$ à distorsion (2 + 4) dans les structures de la volborthite et de $KCu_3^{2+}(OH)_2[(AsO_4)H(AsO_4)]$, et d'un octaèdre $Cu^{2+}\phi_6$ à distorsion (2 + 2 + 2) dans les structures de la bayldonite et de la cyanochroïte, serait due à un effet dynamique de Jahn et Teller, plutôt qu'à un effet statique, comme c'est le cas courant dans les oxysels contenant des octaèdres $Cu^{2+}\phi_6$. C'est la demesmaekerite qui contiendrait le cas le plus convaincant d'un octaèdre $Cu^{2+}\phi_6$ à distorsion (2 + 4).

(Traduit par la Rédaction)

Mots-clés: oxysels de Cu^{2+}, effet de Jahn et Teller, distorsion structurale, distorsion dynamique.

INTRODUCTION

The Cu^{2+} oxysalt minerals have received considerable attention recently (*i.e.*, Eby & Hawthorne 1993, Burns & Hawthorne 1995a, b), primarily because they show considerable structural diversity and are commonly not isostructural with non-Cu^{2+} analogues. In part, the structural diversity may be attributed to the wide range of coordination geometries displayed by Cu^{2+}: six-coordinate octahedral, six-coordinate trigonal-prismatic, five-coordinate square-pyramidal, five-coordinate triangular-bipyramidal and four-coordinate square-planar all occur. Of these, the octahedron is by far the most common coordination polyhedron, and it almost invariably involves a very strong distortion away from holosymmetric octahedral coordination.

The strong distortion of $Cu^{2+}\phi_6$ (ϕ: O^{2-}, OH^-, H_2O) octahedra is due to the Jahn–Teller effect (Jahn & Teller 1937), associated with the degenerate electronic ground state of a d^9 metal in a holosymmetric octahedral field. However, some details of the Jahn–Teller distortion of $Cu^{2+}\phi_6$ octahedra in mineral

[1] Department of Geology, University of Illinois at Urbana-Champaign, 245 Natural History Building, 1301 West Green Street, Urbana, Illinois 61801, U.S.A.
E-mail address: pburns@hercules.geology.uiuc.edu

structures are poorly understood. For example, to first order, the Jahn–Teller theorem leads to the prediction that either a (4 + 2) distortion (four short Cu^{2+}–ϕ equatorial bonds and two long Cu^{2+}–ϕ apical bonds) or a (2 + 4) distortion is equally likely, although examination of crystal structures shows that (4 + 2)-distorted $Cu^{2+}\phi_6$ octahedra occur almost exclusively (Eby & Hawthorne 1993). In rare instances, apparent (2 + 4)-distorted and holosymmetric $Cu^{2+}\phi_6$ octahedra have been reported in mineral structures. To address these apparent anomalies, the details of $Cu^{2+}\phi_6$ octahedral geometries in Cu^{2+} oxysalt structures are considered here.

Jahn–Teller Theory

Screening arguments

Where Cu^{2+} is octahedrally coordinated, the metal d_{xy}, d_{yz} and d_{xz} orbitals are equivalent and involve electron density between the axes containing both the metal ion and the ligands. Both of the d_{z^2} and $d_{x^2-y^2}$ orbitals direct electron density toward the ligands. The octahedral arrangement of ligands around the metal ion splits the five *d*-orbitals into two sets (Fig. 1), one set (t_{2g}) being triply degenerate (corresponding to the copper d_{xy}, d_{yz} and d_{xz} orbitals), and the other (e_g) being doubly degenerate (corresponding to the copper d_{z^2} and $d_{x^2-y^2}$ orbitals). The t_{2g} orbitals are stabilized, and the e_g orbitals are destabilized relative to their energies in a spherical field, the energy difference between the t_{2g} and e_g orbitals being designated Δ_O (Fig. 1). The driving force of the Jahn–Teller distortion of $Cu^{2+}\phi_6$ octahedra results from the unequal occupancies of the two e_g orbitals, which are split by the distortion (Fig. 1). Where the Jahn–Teller distortion occurs, the singly occupied orbital is destabilized by the same energy as the doubly occupied orbital is stabilized, resulting in a net stabilization of energy. Ligand-field arguments (Orgel 1966) show that single occupancy of the d_{z^2} and $d_{x^2-y^2}$ orbitals of Cu^{2+} will result in compressed (2 + 4) and elongated (4 + 2) $Cu^{2+}\phi_6$ octahedra, respectively.

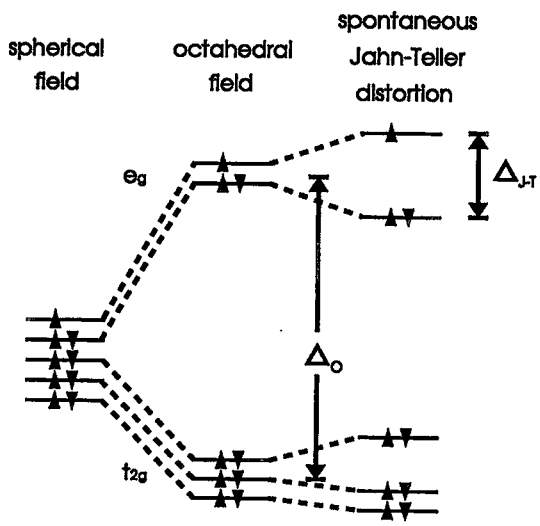

FIG. 1. The electronic energy-levels for Cu^{2+} in a spherical field (left), an octahedral field (middle) and a distorted octahedral field (right).

Ligand-field arguments for a d^9 metal ion in octahedral coordination indicate that a compressed (2 + 4) geometry is equally as likely as an elongated (4 + 2) geometry. However, examination of $^{[6]}Cu$–ϕ bond lengths in Cu^{2+} oxysalt minerals indicates that (4 + 2)-distorted octahedra are very strongly preferred over either the (2 + 4)-distorted or holosymmetric geometries (Eby & Hawthorne 1993). The same observation holds true for Cu^{2+} compounds in general (Hathaway 1984). The details of the Jahn–Teller theory thus are not readily understood using ligand-field theory alone. Various authors have considered additional effects in an attempt to remove these discrepancies; these effects are discussed in the next section.

The dynamic Jahn–Teller effect

Variable-temperature refinements of structures have provided considerable insight into the Jahn–Teller effect associated with a d^9 metal in octahedral coordination. For example, holosymmetric octahedral coordination around $Cu^{2+}\phi_6$ is observed in the structure of $K_2Pb[Cu^{2+}(NO_2)_6]$ at room temperature (Sidgwick 1950, Cullen & Lingafelter 1971), in apparent violation of the Jahn–Teller theorem. At 195 K, the structure is orthorhombic, and the $Cu^{2+}\phi_6$ octahedron is (2 + 4)-distorted (Sidgwick 1950). A (2 + 4)-distorted $Cu^{2+}\phi_6$ octahedron is observed in the structure of $Cs_2Pb[Cu^{2+}(NO_2)_6]$ at room temperature (Massey 1973). The structure is cubic at 420 K, with a holosymmetric $Cu^{2+}\phi_6$ octahedron observed (Mullen *et al.* 1975). When the structure is cooled to 160 K, it becomes monoclinic, with a (4 + 2)-distorted $Cu^{2+}\phi_6$ octahedron (Mullen *et al.* 1975). The temperature-dependent behavior of the octahedral geometries in these and other Cu^{2+} compounds [see Hathaway (1984) for a review] may not be explained using first-order Jahn–Teller effects alone, and the dynamic Jahn–Teller effect must be involved.

Octahedral complexes with an electronic degeneracy in the e_g orbitals, as is the case for $Cu^{2+}\phi_6$, have a single Jahn–Teller active normal mode of vibration of e_g symmetry (Deeth & Hitchman 1986). The even mode of vibration of e_g symmetry is the only mode that can couple with the electronically degenerate ground-state in a cubic system and remove

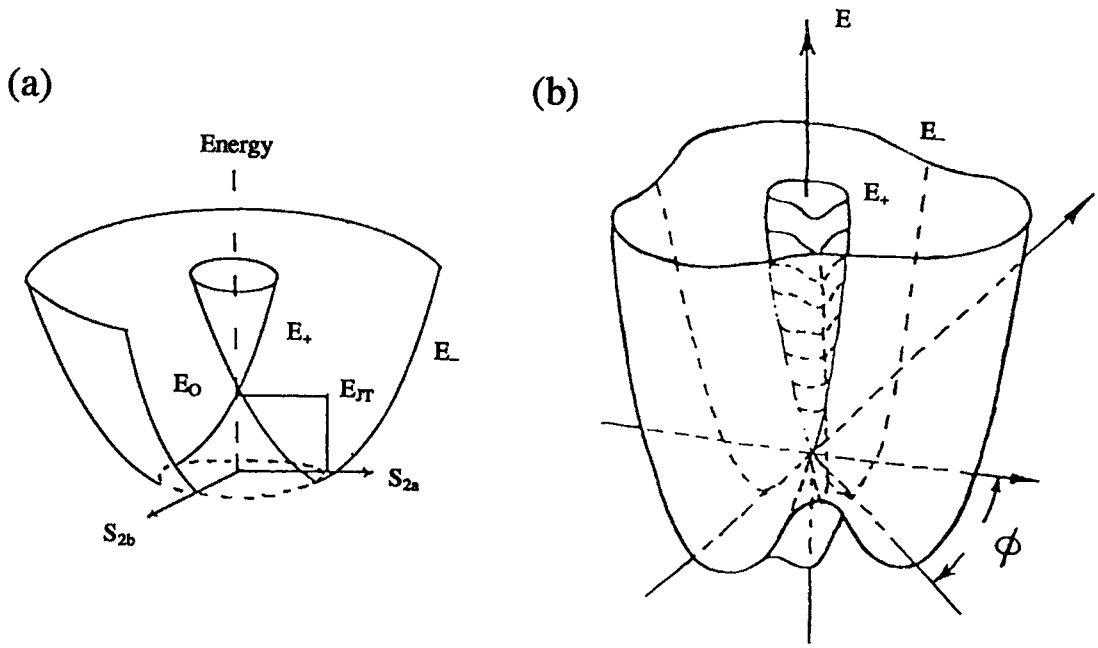

FIG. 2. Mexican-hat potentials: (a) the Mexican-hat potential that results from the coupling of the e_g mode of octahedral vibration with the degenerate electronic state (from Gažo *et al.* 1976). E_O is the energy of a holosymmetric octahedron, E_+ and E_- are the energy surfaces produced by vibronic coupling, E_{JT} is the Jahn–Teller stabilization energy; (b) the warped Mexican-hat potential (from Bersuker 1984).

the orbital degeneracy (Hathaway 1984). Two energy surfaces arise from this coupling (E_- and E_+, Fig. 2a), and take a form known as a *Mexican-hat potential* (Gažo *et al.* 1976). The lower-energy surface of the Mexican-hat potential (E_-) has a potential-energy minimum that is stabilized by E_{JT} relative to the energy of the $Cu^{2+}\phi_6$ octahedron in a holosymmetric configuration (energy E_O). Coupling of the electronic Hamiltonian (for a doubly degenerate state) with the nuclear vibrations gives rise to both linear and non-linear (higher order) terms (Englman 1972). If only linear coupling terms are important, the Mexican-hat potential has cylindrical symmetry (Gažo *et al.* 1976). However, if there is a strong linear coupling and higher-order coupling terms are important, the Mexican hat will be warped, with three energy-minima and three saddlepoints (Bersuker 1984) (Fig. 2b).

The minima in the warped Mexican-hat potential-energy surface (Fig. 2b) may occur at $\phi = 0$, 120 and 240° or at $\phi = 60$, 180 and 300° (Hathaway 1984), depending upon the nature of the higher-order coupling terms. In the first case, the energy minima correspond to (4 + 2)-elongated octahedra, whereas the saddle-points correspond to (2 + 4)-compressed octahedra. In the second case, the energy minima correspond to (2 + 4)-compressed octahedra. Note that in either case, the octahedron can pass from a (4 + 2)-elongated octahedron to a (2 + 4)-compressed octahedron without passing through the energetically unfavorable holosymmetric coordination (Fig. 2b).

Consider the case where the energy minima of the warped Mexican-hat potential occur at $\phi = 0$, 120 and 240°. The energy minima correspond to (4 + 2)-elongated octahedra. This is usually the case, as indicated by the dominance of (4 + 2)-distorted $Cu^{2+}\phi_6$ octahedra in Cu^{2+} oxysalt minerals and compounds in general. Various authors have proposed factors that are likely to cause dominance of the (4 + 2)-distorted arrangement (*e.g.*, Öpik & Pryce 1957, Liehr & Ballhausen 1958, Lohr & Lipscomb 1963, Bacci 1979, Yamatera 1979, Burdett 1980, Deeth & Hitchman 1986); these include: (1) addition of an anharmonic term to the vibrational potential, (2) extension to second order of the electronic terms in the total potential-energy expression, and (3) configuration interaction between the $4s$ and $3d_{z^2}$ metal orbitals. Deeth & Hitchman (1986) suggested that each of these factors is of similar magnitude, and that (1) and (3) favor a (4 + 2)-distortion, whereas (2) favors a (2 + 4)-distortion.

The circular cross-section through the minimum of the potential-energy surface for energy minima at

ϕ = 0, 120 and 240° (Fig. 2b) is given in Figure 3. In this case, the energy maxima correspond to (2 + 4)-compressed octahedra, each of the three energy wells (Fig. 3a) have the same energy, and the energy barriers between the wells have the value *B*. If *B* is less than the thermal energy (*ca.* 200 cm^{-1}, Hathaway 1984), there will be equal populations in each of the three wells. The direction of distortion in any given octahedron will vary continuously as the energy barrier *B* is overcome. As a result, a completely symmetric $Cu^{2+}\phi_6$ octahedron will be observed by (time averaging) crystallographic techniques, as is the case in the structure of $K_2Pb[Cu^{2+}(NO_2)_6]$ at room temperature (Sidgwick 1950) and $Cs_2Pb[Cu^{2+}(NO_2)_6]$ at 420 K (Mullen *et al.* 1975).

In crystals, long-range effects are always present and may result in a further warping of the Mexican-hat surface (Bersuker 1984). Two possibilities then arise: (1) there may be two equivalent wells of lower energy than the third well (Fig. 3b); (2) one well may have a lower energy than the other two wells (Fig. 3c). In (1), if the energy *B* is less than the thermal energy, equal populations will occur in the two lower-energy wells. The two wells involve octahedra that are elongated in different directions, with dynamic interchange between the orientations of the elongated axis. The net result is that an apparent (2 + 4)-compressed octahedron will be observed by crystallographic techniques. By the same reasoning, case (2) will result in an apparently elongated rhombic octahedron, with a (2 + 2 + 2)-distortion [a (2 + 2 + 2) octahedron has two short *trans* Cu–ϕ bonds, two intermediate *trans* Cu–ϕ bonds, and two long *trans* Cu–ϕ bonds].

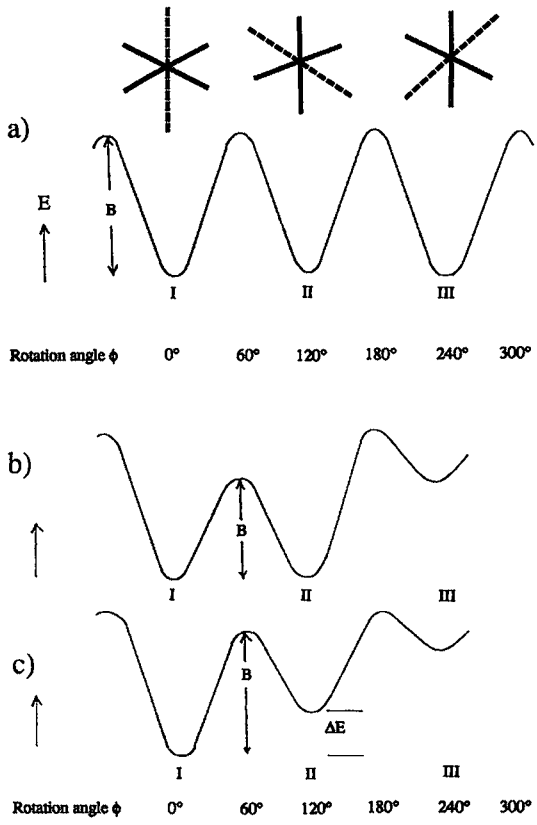

FIG. 3. Circular cross-sections through warped Mexican-hat potentials: (a) three equal-energy wells, (b) two equal-energy wells, and (c) three unequal-energy wells. The definition of ϕ is as in Figure 2; the long bonds in the $Cu^{2+}\phi_6$ octahedra are dashed.

The above observations suggest that both (2 + 4)-compressed and holosymmetric $Cu^{2+}\phi_6$ octahedra observed in the structures of minerals and other phases may in some cases be a result of the dynamic Jahn–Teller effect. It could also be argued that these octahedra are due to averaged static disorder of the octahedral ligands, but the dynamic Jahn–Teller effect is required to rationalize the temperature dependence of $Cu^{2+}\phi_6$ octahedral coordination-geometries in both $K_2Pb[Cu^{2+}(NO_2)_6]$ and $Cs_2Pb[Cu^{2+}(NO_2)_6]$, and in various other Cu^{2+} compounds (Hathaway 1984). As expected, X-ray data collected for these phases also show anisotropic-displacement parameters consistent with dynamically distorted $Cu^{2+}\phi_6$ octahedra. Furthermore, electron-spin-resonance (ESR) spectra for these compounds indicate that (2 + 4)-distorted and holosymmetric $Cu^{2+}\phi_6$ octahedra are both a result of the dynamic Jahn–Teller effect. According to Hathaway *et al.* (1981), there are no compounds that have been conclusively shown to contain *statically* (2 + 4)-distorted or holosymmetric $Cu^{2+}\phi_6$ octahedra. It has been noted, however, that dilute concentrations of $Cu^{2+}\phi_6$ octahedra in a parent structure *may* be (2 + 4)-distorted, as indicated by ESR spectroscopy (*e.g.*, Hitchman *et al.* 1986, Reinen & Krause 1981).

Cooperative Jahn–Teller effects

As shown by crystal-structure refinements, the dynamic Jahn–Teller effect apparently does not occur in most Cu^{2+} oxysalt minerals. In most cases, a static Jahn–Teller effect predominates, with $Cu^{2+}\phi_6$ octahedra trapped in one of the energy wells. However, if two or three of the wells are of about the same energy, directional disorder of the distortion could occur, such that long-range averaging (as occurs in diffraction experiments) will show symmetrical octahedra (three equal wells) or (2 + 4)-compressed octahedra (two equal wells). Cu^{2+} oxysalt minerals usually have (4 + 2)-elongated octahedra, indicating that one energy well is of a lower energy than the other two wells. The directions of elongation of the octahedra are ordered, and this ordering is referred to as the cooperative Jahn–Teller effect (Bersuker 1984).

Ordering of the distortion centers is due to strong electron–phonon coupling that links the effects of adjacent distortion centers.

$Cu^{2+}\phi_6$ Geometries in Cu^{2+} Oxysalt Minerals

Eby (1988) and Eby & Hawthorne (1993) compared $Cu^{2+}\phi_6$ geometries in Cu^{2+} oxysalt minerals. However, over the past few years, high-quality structural data for Cu^{2+} oxysalt minerals have continued to accumulate at the rate of several structures per year. The structures of ninety-one $^{[6]}Cu^{2+}$ oxysalt minerals are considered here, and one hundred and sixty-six symmetrically distinct $Cu^{2+}\phi_6$ octahedra occur in these mineral structures. The following sections consider the stereochemical characteristics of these octahedra. Mixed-ligand $Cu^{2+}\phi_6$ octahedra (ϕ: O^{2-}, OH^-, H_2O and at least one Cl) are considered by Burns & Hawthorne (1995a).

General features of $Cu^{2+}\phi_6$ octahedral geometries

The distribution of Cu–ϕ bond-lengths for all symmetrically distinct $Cu^{2+}\phi_6$ octahedra in Cu^{2+} oxysalt mineral structures is shown in Figure 4. There is a bimodal distribution, with maxima at ~1.95 and ~2.40 Å, reflecting the dominance of (4 + 2)-distorted octahedra. Although most $Cu^{2+}\phi_6$ octahedra in mineral structures are (4 + 2)-distorted, examples of (2 + 4)-distorted and holosymmetric $Cu^{2+}\phi_6$ octahedra also occur. Each subclass of $Cu^{2+}\phi_6$ geometries, *i.e.*, (4 + 2)-distorted, (2 + 4)-distorted and holosymmetric, is dealt with separately in the following sections.

(4 + 2)-distorted $Cu^{2+}\phi_6$ octahedral geometries

By far the most common subclass of $Cu^{2+}\phi_6$ octahedral geometries observed in minerals is the (4 + 2)-distorted octahedron. There are one hundred and fifty-nine symmetrically unique (4 + 2)-distorted octahedra in the structures of ninety different Cu^{2+} oxysalt minerals.

For (4 + 2)-distorted $Cu^{2+}\phi_6$ octahedra, essentially all of the Cu–ϕ_{eq} (eq: equatorial) distances are in the range 1.875 to 2.125 Å, and the Cu–ϕ_{ap} (ap: apical) distances are in the range 2.225 to 3.125 Å. The <Cu–ϕ> distance is 2.150 Å, with a standard deviation of 0.28 Å. The <Cu–ϕ_{eq}> distance is 1.973 Å, and the <Cu–ϕ_{ap}> distance is 2.505 Å. The equatorial bond-lengths span a much smaller range than the apical bond-lengths, with a standard deviation of 0.048 Å compared to 0.205 Å for the apical bond-lengths.

Bond-valence theory (Brown 1981) predicts that distorted coordination-polyhedra will show longer mean bond-lengths than corresponding regular coordination-polyhedra because of the exponential form of the bond-valence interaction. This was shown to be the case for $Cu^{2+}\phi_6$ octahedra by Eby & Hawthorne (1993), who described polyhedral distortion using the parameter Δ:

$$\Delta = \tfrac{1}{6}\,\Sigma[(l_i - l_o)/l_o]^2 \qquad (1)$$

where l_i is a Cu–ϕ distance and l_o is the <Cu–ϕ> distance. The value of Δ for each (4 + 2)-distorted $Cu^{2+}\phi_6$ octahedron is plotted *versus* <Cu–ϕ> in Figure 5. Extrapolation to $\Delta = 0$ gives the expected <Cu–ϕ> distance of 2.083 Å for an undistorted $Cu^{2+}\phi_6$

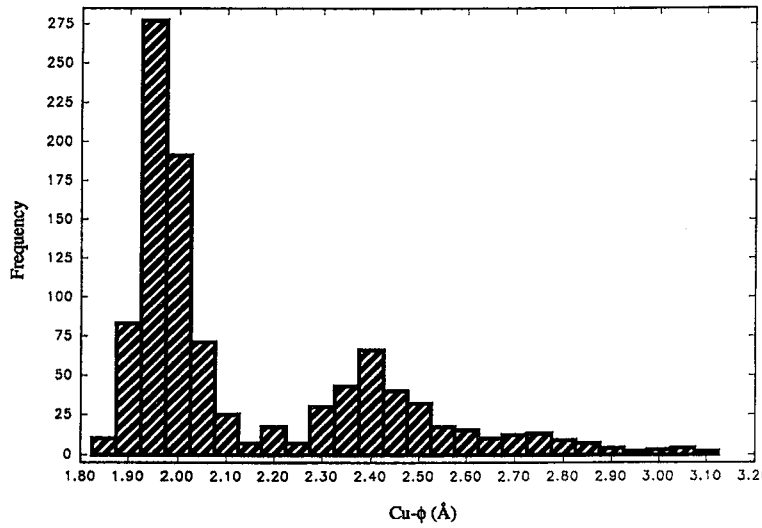

FIG. 4. The distribution of Cu–ϕ bond lengths in all symmetrically distinct $Cu^{2+}\phi_6$ octahedra in Cu^{2+} oxysalt mineral structures.

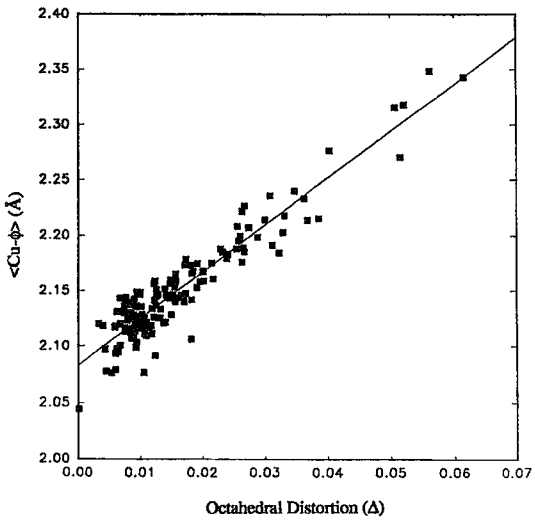

FIG. 5. The <Cu–ϕ> bond length *versus* octahedral distortion (Δ) for (4 + 2)-distorted $Cu^{2+}\phi_6$ octahedra in Cu^{2+} oxysalt minerals. The least-squares line intercept is at <Cu–ϕ> = 2.083 Å for Δ = 0.0.

octahedron, in agreement with the value of 2.084 Å reported by Eby & Hawthorne (1993).

Holosymmetric $Cu^{2+}\phi_6$ octahedra

The occurrence of holosymmetric $Cu^{2+}\phi_6$ octahedra in Cu^{2+} oxysalt minerals is unexpected, as it violates the Jahn–Teller theorem. However, $Cu^{2+}\phi_6$ octahedra with little or no distortion do occur, for example in the structures of lyonsite, buttgenbachite and paratacamite.

Lyonsite: Lyonsite, $Cu_3^{2+}Fe_4^{3+}(VO_4)_6$, is a rare high-temperature fumarolic sublimate described by Hughes *et al.* (1987). The structure of lyonsite is based on a pseudohexagonal close-packed array of oxygen atoms, and contains two symmetrically distinct $Cu^{2+}\phi_6$ polyhedra, one of which [*Cu*(2)] shows a very unusual $Cu^{2+}\phi_6$ coordination: a distorted trigonal-prism. A similar $Cu^{2+}\phi_6$ coordination polyhedron occurs in claringbullite (Burns *et al.* 1995), buttgenbachite (Fanfani *et al.* 1973) and connellite (McLean & Anthony 1972). The *Cu*(1) site in lyonsite involves a $Cu^{2+}\phi_6$ octahedron that is only very weakly distorted [*Cu*(1)–*O*(1) × 2 = 2.031(5), *Cu*(1)–*O*(1) × 2 = 2.030(5), *Cu*(1)–*O*(6) × 2 = 2.070(7) Å]. Further examination of the lyonsite structure shows that adjacent $Cu^{2+}(1)\phi_6$ octahedra share faces, with the associated *Cu*(1) positions only 2.455 Å apart. Such a configuration suggests that adjacent *Cu*(1) sites are probably not both occupied; site-scattering refinement shows the *Cu*(1) site to be half-occupied, consistent with this situation (Hughes *et al.* 1987).

If a site is partly occupied, as is the case for the *Cu*(1) site in lyonsite, the local atomic configurations are expected to be very different than if the site is fully occupied or vacant. The long-range average configuration measured by X-ray diffraction consists of the sum of these two configurations, and may not resemble either of the local configurations very closely. The fact that regular $Cu^{2+}\phi_6$ configurations are not found where a site is completely filled by Cu^{2+} suggests that the long-range average observed in the structure of lyonsite (and buttgenbachite, see below) consists of distorted $Cu^{2+}\phi_6$ and distorted $\square\phi_6$ configurations that *average* to regular octahedral geometry. Adding to the uncertainty as to the precise nature of the *Cu*(1) site is the approximately 50% vacancy and the marked anisotropy of the electron density at the *Cu*(1) site. The electron-density anisotropy suggests that the room-temperature structure may represent a space average of disordered *Cu*(1) positions within the octahedron (Hughes *et al.* 1987). Although it is not possible to directly prove this model, the preponderance of partly filled sites in holosymmetric $Cu^{2+}\phi_6$ configurations suggests that this is the case.

Buttgenbachite: The structure of buttgenbachite, $Cu_{36.6}^{2+}Cl_{6.7}(NO_3)_{2.6}(OH)_{63.2}\cdot 2.1H_2O$ (Fanfani *et al.* 1973), contains an infinite three-dimensional framework of Cu^{2+} polyhedra with large channels containing (NO_3) and Cl. There are five symmetrically distinct Cu^{2+} sites. Three of these sites are octahedrally coordinated and show typical (4 + 2)-distortion (although two contain mixed ligands; see Burns & Hawthorne 1995a), whereas the fourth Cu^{2+} cation is in square-planar coordination. The fifth Cu^{2+} site is in holosymmetric octahedral coordination, with *Cu*(5)–*OH*(2) × 6 = 2.210(7) Å. According to site-scattering information, this site is only one-third occupied. The argument given for lyonsite also applies to buttgenbachite: the regular arrangement observed around the *Cu*(5) site is probably a superposition of distorted $Cu^{2+}\phi_6$ and $\square\phi_6$ configurations.

Paratacamite: Paratacamite is one of the polymorphic forms of $Cu_2^{2+}(OH)_3Cl$. The structure has rhombohedral symmetry, with a distinct substructure (Fleet 1975). The structure contains four symmetrically distinct Cu^{2+} positions. Two of these positions are in (4 + 2)-distorted mixed-ligand octahedral coordination (see Burns & Hawthorne 1995a), and the third Cu^{2+} site has (2 + 4)-distorted octahedral coordination. The *Cu*(1) site contains one-sixteenth of the copper in the paratacamite structure, and occurs on a $\bar{3}$ axis; the octahedron is holosymmetric, with *Cu*(1)–O × 6 = 2.12 Å. This site is 100% occupied, unlike the holosymmetric octahedron in buttgenbachite or the near-holosymmetric octahedron in lyonsite. The <Cu–ϕ> value of 2.12 Å is somewhat longer

than the expected <Cu–ϕ> distance of 2.083 Å for an undistorted $Cu^{2+}\phi_6$ octahedron. Fleet (1975) reported the structure of a natural specimen of paratacamite, but did not report a chemical composition. If the octahedral site is occupied by Zn^{2+}, the average octahedral distance expected would be 2.10 Å (*i.e.*, 1.36 Å + 0.74 Å: Shannon 1976). The existence of zinc-rich paratacamite was reported by Kracher & Pertlik (1983), and electron-microprobe analysis of a crystal of paratacamite from the same sample as studied by Fleet (1975) showed it to contain 2.4 wt% Zn [Jambor *et al.* 1996, Embrey & Jones (in Kracher & Pertlik 1983)]. Grice *et al.* (1996) reported the structure of clinoatacamite, $Cu_2(OH)_3Cl$ with no detectable Zn, and showed that the structure has the same topology as paratacamite, but that it has monoclinic symmetry. In the clinoatacamite structure, all Cu^{2+} octahedra show the usual Jahn–Teller distortion (Grice *et al.* 1996). Jambor *et al.* (1996) synthesized crystals of $(Cu_{2-x}Zn_x)(OH)_3Cl$ composition; $Cu_2(OH)_3Cl$ was found to have the monoclinic structure, whereas crystals with more than 6 mol.% Zn have the rhombohedral structure. Thus, there is considerable evidence that indicates that Zn is required to stabilize the paratacamite structure, but crystals with only 2.4 wt% Zn have the rhombohedral structure, demonstrating that only about one-half of the holosymmetric octahedral site in the paratacamite structure need contain zinc.

Synthetic compounds: There are no well-documented examples of holosymmetric $Cu^{2+}\phi_6$ octahedra in mineral structures, as predicted by the Jahn–Teller theorem. Holosymmetric $Cu^{2+}\phi_6$ octahedra have been observed in certain synthetic structures by crystallographic techniques. One such example occurs in $[Cu^{2+}(H_2O)_6](BrO_3)_2$, where the <Cu–ϕ> distance is 2.079 Å (Blackburn *et al.* 1991), a value in good agreement with the predicted <Cu–ϕ> distance of 2.083 Å for an undistorted $Cu^{2+}\phi_6$ octahedron. However, the holosymmetric octahedron observed in $[Cu^{2+}(H_2O)_6](BrO_3)_2$, as well as all other holosymmetric Cu^{2+} octahedra (there are six known), is attributed to a dynamic Jahn–Teller effect that persists at room temperature (Blackburn *et al.* 1991, Hathaway 1984). Supporting evidence comes from anisotropic-displacement parameters, variable-temperature refinements of the structure, and measurements by ESR spectroscopy (Blackburn *et al.* 1991, Hathaway 1984).

(2 + 4)-distorted $Cu^{2+}\phi_6$ octahedra

Five (2 + 4)-distorted $Cu^{2+}\phi_6$ octahedra occur in the structures of campigliaite, paratacamite, demesmaekerite and volborthite. Hathaway *et al.* (1981) suggested that genuine (2 + 4)-distorted $Cu^{2+}\phi_6$ octahedra do not occur in Cu^{2+} compounds. Most (or all) examples of (2 + 4)-distorted $Cu^{2+}\phi_6$ octahedra have been shown to be time-averaged results of the dynamic Jahn–Teller effect. These apparent (2 + 4)-distorted $Cu^{2+}\phi_6$ octahedra result from the time averaging of (4 + 2)-distorted octahedra aligned in two directions. However, some spectroscopists have postulated statically (2 + 4)-distorted $Cu^{2+}\phi_6$ octahedra in some Cu^{2+}-doped systems (Hitchman *et al.* 1986, Reinen & Krause 1981) from ESR measurements. As (2 + 4)-distorted $Cu^{2+}\phi_6$ octahedra are rare (or non-existent) in concentrated Cu^{2+} compounds, it is appropriate to consider each of the mineral examples in some detail.

TABLE 1. BOND-LENGTHS (Å) OF (2+4)-DISTORTED $Cu^{2+}\phi_6$ OCTAHEDRA IN MINERALS

Mineral	Bonds				Reference
Volborthite	*Cu*(1)	*O*(2): 2.172(4) x4	*O*(4): 1.945(4) x2		1
Demesmaekerite	*Cu*(1)	*O*(8): 2.21(2) x2 *O*(9): 2.21(1) x2	*OH*(1): 1.93(2) x2		2
Paratacamite*	*Cu*(2)	*O*(2): 2.19 x2 *O*(3): 2.20 x2	*O*(1): 1.93 x2		3
Campigliaite	*Cu*(1)	*O*(1): 2.22(5) *O*(3): 2.37(5)	*O*(4): 2.34(5) *O*(3): 2.42(5)	*O*(4): 1.94(5) *O*(2): 1.93(5)	4
	Cu(3)	*O*(2): 2.17(5) *O*(5): 2.29(5)	*O*(8): 2.21(5) *O*(3): 2.41(5)	*O*(7): 1.84(5) *O*(1): 1.99(5)	
$KCu_3^{2+}(OH)_2[(AsO_4)H(AsO_4)]$**	*Cu*(1)	*O*(3): 2.186(1) x4	*OH*: 1.899(2) x2		5

* Standard deviations were not given by the original author.
** Not a mineral
References: 1: Basso *et al.* (1988); 2: Ginderow & Cesbron (1983); 3: Fleet (1975); 4: Sabelli (1982); 5: Effenberger (1989).

Campigliaite: The structure of campigliaite, $Cu_4^{2+}Mn^{2+}(SO_4)(OH)_6{\cdot}4H_2O$, contains sheets of $Cu^{2+}\phi_6$ octahedra interconnected through SO_4 tetrahedra and hydrogen bonding. The crystal structure (Sabelli 1982) is of low precision owing to the poor quality of the crystal and the presence of polysynthetic twinning. Both the *Cu*(1) and *Cu*(3) sites seem to be in (2 + 4)-distorted octahedral coordination (Table 1). However, it is likely that the observed octahedra are twin-averaged, rather than real (2 + 4)-distorted octahedra.

Paratacamite: The structure of paratacamite (Fleet 1975) was discussed in the previous section with reference to the *Cu*(1) site, which is in a holosymmetric octahedral environment. It was pointed out that the structure of paratacamite may contain significant amounts of Zn, and that the holosymmetric octahedron may contain some Zn. The paratacamite structure also contains one (2 + 4)-distorted $Cu^{2+}\phi_6$ octahedron *Cu*(2) (Table 1). As this (2 + 4)-distorted octahedral geometry is very similar to that observed in the structure of volborthite and demesmaekerite (Table 1), it seems likely that the *Cu*(2) site does contain Cu^{2+}.

Demesmaekerite: The structure of demesmaekerite, $Pb_2Cu_5^{2+}(SeO_3)_6(UO_2)_2(OH)_6{\cdot}2H_2O$ (Ginderow & Cesbron 1983), consists of layers of $[Cu^{2+}(O,OH,H_2O)_6]$ octahedra parallel to (010), cross-linked by oblique chains of corner-sharing ($U\phi_7$) and (SeO_3) polyhedra. The structure contains three symmetrically distinct Cu^{2+} sites, two of which are in octahedral coordination with (4 + 2)-distorted geometries. The *Cu*(1) site lies on a center of symmetry, and shows a (2 + 4)-distorted $Cu^{2+}\phi_6$ octahedral geometry (Table 1). Note that this configuration is *not* a requirement of the site symmetry.

Volborthite: The structure of volborthite, $Cu_3^{2+}(OH)_2V_2O_7{\cdot}2H_2O$ (Basso *et al.* 1988), contains sheets of edge-sharing $Cu^{2+}\phi_6$ octahedra. These sheets of octahedra may be derived from a $Mg(OH)_2$ (brucite) layer in which 25% of the octahedral positions are vacant. VO_4 tetrahedra link to each side of the sheet, and bonding between adjacent sheets is through the apical atoms of oxygen of opposing VO_4 tetrahedra and through hydrogen bonding associated with the interstitial H_2O groups.

The structure of volborthite contains two symmetrically distinct Cu^{2+} sites. The *Cu*(2) site occurs at a center of symmetry, and is surrounded by a (4 + 2)-distorted octahedron. The *Cu*(1) site has point symmetry 2/*m*, and the *Cu*(1) octahedron is (2 + 4)-distorted (Table 1). The chemical composition of the material used for the structure study (Basso *et al.* 1988) rules out substitution of another cation at the *Cu*(1) site. Note that the (2 + 4)-distorted geometries in volborthite, paratacamite and demesmaekerite (Table 1) are very similar.

$KCu_3^{2+}(OH)_2[(AsO_4)H(AsO_4)]$: Effenberger (1989) reported a (2 + 4)-distorted $Cu^{2+}\phi_6$ octahedron in the structure of $KCu_3^{2+}(OH)_2[(AsO_4)H(AsO_4)]$, which has not yet been described as a mineral. This material crystallizes in the space group *C*2/*m*, and its structure is closely related to that of volborthite. The structure contains the same sheets of octahedra and tetrahedra as volborthite, with AsO_4 tetrahedra replacing the VO_4 tetrahedra. However, unlike volborthite, adjacent sheets are offset, with intersheet bonding provided by 10-coordinated K and hydrogen bonds. The *Cu*(1) position, which has 2/*m* symmetry, is at the center of a (2 + 4)-distorted octahedron (Table 1). The *Cu*(1)–ϕ bond lengths are similar to those in volborthite, but the $\langle Cu(1)\text{–}\phi_{eq}\rangle$ distance is slightly longer, and the $\langle Cu(1)\text{–}\phi_{ap}\rangle$ distance, significantly shorter, than the corresponding values in volborthite (Table 1). The *Cu*(2) site is in (4 + 2)-distorted octahedral coordination, similar to that observed in the volborthite structure.

The occurrence of a (2 + 4)-distorted $Cu^{2+}\phi_6$ octahedral geometry in the structures of both volborthite and $KCu_3^{2+}(OH)_2[(AsO_4)H(AsO_4)]$ suggests that the octahedral geometry results from connectivity constraints associated with the particular sheets of octahedra and tetrahedra that occur in both structures. Possibly a (2 + 4)-distorted octahedron is energetically preferred over a (4 + 2)-distorted octahedron at the *Cu*(1) site, with this very unusual situation somehow tied to the connectivity requirements of the sheets. However, the structural arrangement in bayldonite suggests otherwise.

Bayldonite: Bayldonite, $Cu_3^{2+}Pb(AsO_4)_2(OH)_2$ (Ghose & Wan 1979), space group *C*2/*c*, has a unit cell that is very similar to those of volborthite and $KCu_3^{2+}(OH)_2[(AsO_4)H(AsO_4)]$ (Table 2). The bayldonite structure contains sheets of $Cu^{2+}\phi_6$ octahedra and AsO_4 tetrahedra that are graphically identical to the sheets of octahedra and tetrahedra in volborthite and $KCu_3^{2+}(OH)_2[(AsO_4)H(AsO_4)]$. Adjacent sheets of octahedra and tetrahedra in the structure of bayldonite are connected through irregular $Pb^{2+}\phi_8$ polyhedra and hydrogen bonding. The *c* dimension of bayldonite is double that of volborthite and $KCu_3^{2+}(OH)_2[(AsO_4)H(AsO_4)]$, and there are three distinct Cu^{2+} sites, each of which is located at a center of symmetry. The $Cu^{2+}\phi_6$ bond lengths in bayldonite are compared to those in volborthite and $KCu_3^{2+}(OH)_2[(AsO_4)H(AsO_4)]$ in Table 2. Note that the *Cu*(2) site in bayldonite is related to the *Cu*(1) sites in volborthite and $KCu_3^{2+}(OH)_2[(AsO_4)H(AsO_4)]$, but the ligand arrangement is not (2 + 4)-distorted. Instead, the Cu(2) octahedron in bayldonite shows an elongated-rhombic distortion, best referred to as a (2 + 2 + 2)-distorted octahedron.

The (2 + 4)-distorted $Cu^{2+}\phi_6$ octahedra observed in Cu^{2+} oxysalt minerals are derived from X-ray diffraction data, and as such may be the result of: (i) the presence of a statically (2 + 4)-distorted octahedron, (ii) the dynamic time-averaging of two non-aligned (4 + 2)-distorted octahedra, (iii) the static disorder of (4 + 2)-distorted octahedra. We propose that the (2 + 4)-distorted $Cu^{2+}\phi_6$ octahedra in the structures of volborthite and $KCu_3^{2+}(OH)_2[(AsO_4)H(AsO_4)]$, and the (2 + 2 + 2)-distorted octahedron in the structure of bayldonite, are the result of a dynamic Jahn–Teller effect. Supporting arguments are given below, but first it is necessary to consider (2 + 2 + 2)-distorted $Cu^{2+}\phi_6$ geometries in more detail.

(2 + 2 + 2)-Distorted $Cu^{2+}\phi_6$ Octahedra in Cu^{2+} Oxysalt Minerals

The ligand-field arguments presented above indicate that either a (4 + 2) or (2 + 4) tetragonal distortion of the $Cu^{2+}\phi_6$ octahedral environment will remove the energetically degenerate electronic state and stabilize the octahedron. However, examination of $Cu^{2+}\phi_6$ octahedra in Cu^{2+} oxysalt minerals shows that tetragonally distorted octahedra are rare: to date, only five such

TABLE 2. COMPARISON OF UNIT-CELL PARAMETERS AND BOND-LENGTHS FOR $Cu^{2+}\phi_6$ OCTAHEDRA FOR VOLBORTHITE, BAYLDONITE AND $KCu_3^{2+}(OH)_2[(AsO_4)H(AsO_4)]$

		a (Å)	b (Å)	c (Å)	β (°)	Space Group	Ref.
Volborthite $Cu_3^{2+}(OH)_2V_2O_7.2H_2O$		10.610(2)	5.866(1)	7.208(1)	95.04(2)	*C2/m*	1
Bayldonite $Cu_3^{2+}Pb(AsO_4)_2(OH)_2$		10.147(2)	5.892(1)	14.081(2)	106.05(1)	*C2/c*	2
$KCu_3^{2+}(OH)_2[(AsO_4)H(AsO_4)]$		10.292(5)	5.983(3)	7.877(4)	117.86(2)	*C2/m*	3
			Octahedral bond distances				
Volborthite	*Cu*(1)	1.945(4) x2	*Cu*(2)	1.922(3) x2			
		2.172(4) x4		2.031(3) x2			
				2.414(3) x2			
Bayldonite	*Cu*(2)	1.878(7) x2	*Cu*(3)	1.924(9) x2	*Cu*(1)	1.891(7) x2	
		2.087(10) x2		2.000(8) x2		2.039(8) x2	
		2.272(9) x2		2.454(8) x2		2.423(10) x2	
$KCu_3^{2+}(OH)_2[(AsO_4)H(AsO_4)]$	*Cu*(1)	1.899(2) x2	*Cu*(2)	1.934(1) x2			
		2.186(1) x4		2.000(1) x2			
				2.428(1) x2			

References: 1: Basso *et al.* (1988); 2: Ghose & Wan (1979); 3: Effenberger (1989).

$Cu^{2+}\phi_6$ octahedra occur in minerals.

Apical and equatorial Cu–ϕ distortion parameters may be defined individually as:

$$\Delta_{ap} = \tfrac{1}{2}\,\Sigma[(l_{ap,i}-l_{ap,o})/l_{ap,o}]^2 \quad (2)$$

$$\Delta_{eq} = \tfrac{1}{4}\,\Sigma[(l_{eq,i}-l_{eq,o})/l_{eq,o}]^2 \quad (3)$$

where l_o is the average bond-length. The values of Δ_{ap} and Δ_{eq} for all (4 + 2)-distorted $Cu^{2+}\phi_6$ octahedra in minerals are shown in Figure 6. For ranges of Δ_{eq} from 0 to 0.00075, there is a considerable range of Δ_{ap} observed, *i.e.*, from 0 to 0.023. However, for values of Δ_{eq} ranging from 0.00075 to 0.003, there is generally a very narrow range of Δ_{ap}.

Of the one hundred and fifty-nine (4 + 2)-distorted $Cu^{2+}\phi_6$ octahedra in Cu^{2+} oxysalt minerals, forty-two occur on a center of symmetry. Each of these octahedra must have $\Delta_{ap} = 0.0$, and plot along the horizontal axis in Figure 6. In many of these cases, the centrosymmetric $Cu^{2+}\phi_6$ octahedra show very large values of Δ_{eq}. Note also that there are several occurrences of $Cu^{2+}\phi_6$ octahedra that have large values of Δ_{eq}, but low values of Δ_{ap} that are not on centers of symmetry (*i.e.*, $\Delta_{ap} \neq 0.0$).

The $Cu^{2+}\phi_6$ octahedra with high values of Δ_{eq} and low values of Δ_{ap} are rhombically elongated octahedra, and typically have two short *trans* Cu–ϕ_{eq} distances, two long *trans* Cu–ϕ_{ap} distances and two intermediate *trans* Cu–ϕ_{eq} distances. Such a distortion is best referred to as a (2 + 2 + 2) distortion and can be considered as a subclass of the (4 + 2)-distorted $Cu^{2+}\phi_6$ octahedra, as the two intermediate Cu–ϕ_{eq} distances are almost invariably closer to the short Cu–ϕ_{eq} distances than to the long Cu–ϕ_{ap} distances. Examples of (2 + 2 + 2)-distorted $Cu^{2+}\phi_6$ octahedra in minerals are given in Table 3, which contains only (2 + 2 + 2)-distorted octahedra in which the average long Cu–ϕ_{eq} distance is greater than 0.10 Å longer than the average short Cu–ϕ_{eq} distance.

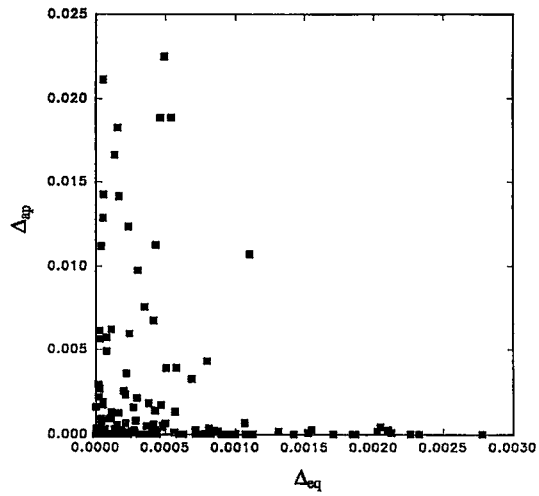

FIG. 6. Apical and equatorial bond-length distortion parameters for (4 + 2)-distorted $Cu^{2+}\phi_6$ octahedra in Cu^{2+} oxysalt minerals; note the different scales on each axis.

TABLE 3. EXAMPLES OF (2+2+2)-DISTORTED $Cu^{2+}\phi_6$ OCTAHEDRA OBSERVED IN Cu^{2+} OXYSALT MINERALS; BOND-LENGTHS IN Å

							Ref.	Δ_T
Octahedra on a center of symmetry								
Bayldonite	1.878	x2	2.087	x2	2.272	x2	1	0.910
	1.891	x2	2.039	x2	2.423	x2		0.881
Cyanochroite	1.944	x2	2.069	x2	2.279	x2	2	0.923
Turquois	1.915	x2	2.109	x2	2.422	x2	3	0.888
Chalcosiderite	1.914	x2	2.079	x2	2.484	x2	4	0.875
Dolerophanite	1.992	x2	2.070	x2	2.526	x2	5	0.884
Volborthite	1.922	x2	2.031	x2	2.414	x2	6	0.889
Ludjibaite	1.918	x2	2.04	x2	2.578	x2	7	0.857
Vauquelinite	1.94	x2	2.06	x2	2.44	x2	8	0.889
Chalcocyanite	1.916	x2	2.049	x2	2.373	x2	9	0.897
Cornubite	1.911	x2	2.031	x2	2.467	x2	10	0.876

Octahedra not on a center of symmetry							Ref.
Campigliaite	1.86	2.00	2.08	2.09	2.39	2.47	11
Kamchatkite	1.86	1.98	2.03	2.04	2.37	2.47	12
Conichalcite	1.95	1.95	2.04	2.09	2.38	2.38	13
Calciovolborthite	1.906	1.909	2.056	2.071	2.337	2.415	14
Duftite	1.91	1.94	2.10	2.11	2.29	2.35	15
Malachite	1.918	1.915	2.049	2.115	2.372	2.369	16
	1.898	1.911	1.996	2.055	2.509	2.642	
Pseudomalachite	1.884	1.884	1.974	1.985	2.395	2.755	17
Antlerite	1.906	1.923	2.024	2.033	2.344	2.414	18
Demesmaekerite	1.95	1.95	2.04	2.07	2.38	2.39	19
Fornacite	1.84	1.95	2.02	2.08	2.36	2.46	20
Devillite	1.90	2.00	2.10	2.12	2.37	2.37	21
	1.89	1.93	2.07	2.11	2.38	2.43	
	1.85	1.91	1.99	2.05	2.44	2.49	

References: 1: Ghose & Wan (1979); 2: Robinson & Kennard (1972); 3: Cid-Dresdner (1965); 4: Giuseppetti *et al.* (1989); 5: Effenberger (1985); 6: Basso *et al.* (1988); 7: Shoemaker *et al.* (1981); 8: Fanfani & Zanazzi (1968); 9: Wildner & Giester (1988); 10: Sieber *et al.* (1984); 11: Sabelli (1982); 12: Varaksina *et al.* (1990); 13: Qurashi & Barnes (1963); 14: Basso *et al.* (1989); 15: Effenberger & Pertlik (1988); 16: Zigan *et al.* (1977); 17: Shoemaker *et al.* (1977); 18: Hawthorne *et al.* (1989); 19: Ginderow & Cesbron (1983); 20: Cocco *et al.* (1967); 21: Sabelli & Zanazzi (1972).

For centrosymmetric (2 + 2 + 2)-distorted $Cu^{2+}\phi_6$ octahedra, the degree to which a (2 + 2 + 2)-distortion is present is conveniently given by the parameter Δ_T where:

$$\Delta_T = [(Cu\text{–}\phi_{eq,short}) + (Cu\text{–}\phi_{eq,intermed.})] / [(Cu\text{–}\phi_{eq,intermed.}) + (Cu\text{–}\phi_{ap})] \quad (4)$$

Values of Δ_T (Table 3) range from 0.857 in the structure of lubjibaite to a maximum of 0.923 in cyanochroite; note that cyanochroite and bayldonite are the only Cu^{2+} oxysalt minerals that contain (2 + 2 + 2)-distorted $Cu^{2+}\phi_6$ octahedra with $\Delta_T > 0.90$.

The Mexican-hat potential for the coupling of the e_g vibrational modes with the electronic state of $Cu^{2+}\phi_6$ is given in Figure 2, and is discussed above. The three possible types of circular cross-sections through the minimum of the potential-energy surface of Figure 2 are given in Figure 3. The energy minima occur at ϕ = 0, 120 and 240°, and positions I, II and III correspond to a (4 + 2)-distorted $Cu^{2+}\phi_6$ octahedron elongated in each of the three possible axial directions. If the energy barrier B is less than the thermal energy, a dynamic interchange of elongation directions of the (4 + 2)-distorted octahedron will continually occur as the energy barrier is overcome. The $Cu^{2+}\phi_6$ geometry observed by crystallographic techniques will be a time-averaged geometry. Depending on the relative energies of the wells, either a holosymmetric, (2 + 4)-distorted or a rhombically elongated octahedron [(2 + 2 + 2)-distorted] will be observed.

The structures of copper Tutton's salts show dynamic Jahn–Teller effects. Considerable variable-temperature structural work has been done for $(NH_4)_2Cu^{2+}(H_2O)_6(SO_4)_2$, with the structure studied at 295 K (Webb *et al.* 1965, Montgomery & Lingafelter 1966, Brown & Chibambaram 1969), 203 and 123 K (Alcock *et al.* 1984). The room-temperature structure contains a $Cu^{2+}\phi_6$ octahedron of rhombically elongated octahedral geometry [a (2 + 2 + 2) distortion] (Table 4). This strong (2 + 2 + 2) distortion suggests that the octahedron may be a result of the dynamic Jahn–Teller effect involving two energy wells of similar but unequal energies, and a third well of considerably higher energy. The octahedron is elongated in the *Cu–O*(7) direction most of the time, but the energy well corresponding to elongation in the *Cu–O*(8) direction is also significantly occupied, and a dynamic interchange between these two distortion directions occurs. The temperature-dependent nature of the Cu–ϕ bond-lengths in the $(NH_4)_2Cu^{2+}(H_2O)_6(SO_4)_2$ structure (Table 4) indicates that a dynamic Jahn–Teller effect does occur in this structure (Alcock *et al.* 1984). Continued cooling results in a steady increase of the *Cu–O*(7) distance, a steady decrease in the *Cu–O*(8) distance, and no significant change in the *Cu–O*(9) distance (Table 4).

The structures of some other copper Tutton's salts also have been reported. These include $K_2Cu^{2+}(H_2O)_6(SO_4)_2$ (Robinson & Kennard 1972), $Rb_2Cu^{2+}(H_2O)_6(SO_4)_2$ (Van der Zee *et al.* 1972, Smith *et al.* 1975), $Cs_2Cu^{2+}(H_2O)_6(SO_4)_2$ (Shields & Kennard 1972) and $Tl_2Cu^{2+}(H_2O)_6(SO_4)_2$ (Shields *et al.* 1972);

TABLE 4. OCTAHEDRAL BOND-LENGTHS (Å) IN $(NH_4)_2Cu^{2+}(H_2O)_6(SO_4)_2$ AND $(M^+)_2Cu^{2+}(H_2O)_6(SO_4)_2$, M^+ = K, Rb, Cs, Tl

	$(NH_4)_2Cu^{2+}(H_2O)_6(SO_4)_2$		
	295 K	203 K	123 K
Cu-O(7)	2.219(5)	2.250(2)	2.278(2)
Cu-O(8)	2.095(5)	2.041(2)	2.012(1)
Cu-O(9)	1.961(5)	1.967(2)	1.970(1)
Ref.	1	2	2

	$(M^+)_2Cu^{2+}(H_2O)_6(SO_4)_2$				
	K	Rb	Rb(77 K)	Cs	Tl
Cu-O(8)	2.278(2)	2..307(3)	2.317(5)	2.315(5)	2.317(5)
Cu-O(7)	2.069(3)	2.031(3)	2.000(5)	2.004(4)	2.017(4)
Cu-O(9)	1.943(3)	1.957(3)	1.978(5)	1.966(5)	1.957(5)
Ref.	3	4	5	6	7

References: 1: Montgomery & Lingafelter (1966); 2: Alcock *et al.* (1984); 3: Robinson & Kennard (1972); 4: Van der Zee *et al.* (1972); 5: Smith *et al.* (1975); 6: Shields & Kennard (1972); 7: Shields *et al.* (1972).

of these, $K_2Cu^{2+}(H_2O)_6(SO_4)_2$ is the mineral cyanochroite. The bond lengths for the $Cu^{2+}\phi_6$ octahedron in each of these structures are included in Table 4. Note that the long Cu–O bond is to $O(8)$ in each case rather than to $O(7)$ as in $(NH_4)_2Cu^{2+}(H_2O)_6(SO_4)_2$.

Each of the $(M^+)_2Cu^{2+}(H_2O)_6(SO_4)_2$ structures contain a rhombically elongated $Cu^{2+}\phi_6$ octahedron, *i.e.*, a (2 + 2 + 2)-distorted octahedron. Alcock *et al.* (1984) suggested that the Cs salt probably contains a static (2 + 2 + 2)-distorted $Cu^{2+}\phi_6$ octahedron, with only the lowest-energy well of the potential occupied. They indicated that the $Cu^{2+}\phi_6$ octahedron in the Rb salt has a small but significant dynamic component, as apparently verified by the low-temperature determination of the structure. Alcock *et al.* (1984) suggested that the K salt (cyanochroite) has a considerable dynamic component, with significant thermal population of the two lower-energy wells. Variable-temperature data for the K salt are not available, but comparison of the $Cu^{2+}\phi_6$ geometries in $(NH_4)_2Cu^{2+}(H_2O)_6(SO_4)_2$ and $(M^+)_2Cu^{2+}(H_2O)_6(SO_4)_2$ suggests the presence of a significant dynamic component in $K_2Cu^{2+}(H_2O)_6(SO_4)_2$.

Possible Dynamic Jahn–Teller Effects in Minerals

Most Cu^{2+} oxysalt minerals and Cu^{2+} compounds contain (4 + 2)-distorted $Cu^{2+}\phi_6$ octahedra that show little or no evidence of a dynamic Jahn–Teller component. As minerals are typically quite stable, it has generally been assumed that dynamic Jahn–Teller effects will not occur in their structures. However, the arguments developed here suggest otherwise. The presence of (2 + 4)-distorted and (2 + 2 + 2)-distorted $Cu^{2+}\phi_6$ octahedra in mineral structures suggests that some may show dynamic Jahn–Teller effects. As a dynamic Jahn–Teller effect may lead to observation of each of these coordination geometries, care must be taken to determine whether a static or dynamic Jahn–Teller effect is observed.

Recognition of dynamic Jahn–Teller $Cu^{2+}\phi_6$ octahedra

Cu^{2+} oxysalt minerals containing (2 + 4)- or (2 + 2 + 2)-distorted $Cu^{2+}\phi_6$ octahedra should be investigated further to determine if the configuration is static, dynamic or a result of static disorder. There are three possible means of obtaining this information: (i) variable-temperature crystallographic studies, (ii) crystal-structure refinement followed by the study of anisotropic-displacement parameters, and (iii) electron-spin-resonance (ESR) spectroscopy.

Possible dynamically distorted $Cu^{2+}\phi_6$ octahedra

Several mineral structures contain $Cu^{2+}\phi_6$ octahedra that may be dynamically distorted. Examples are considered in the following sections, and although a strong case may be made for the presence of dynamically distorted $Cu^{2+}\phi_6$ octahedra, further verification by variable-temperature structure refinement is desirable. However, in most cases, the limited thermal stability of these hydrous phases is likely to prevent such studies.

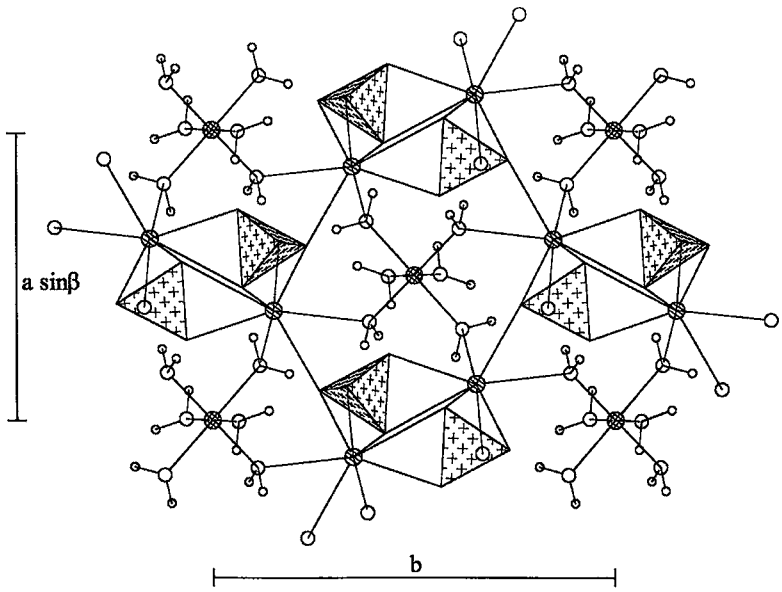

FIG. 7. The structure of cyanochroite, $K_2Cu^{2+}(H_2O)_6(SO_4)_2$, projected onto (001). Cu atoms are shown as cross-hatched circles, K atoms as circles shaded with parallel lines, $S\phi_4$ tetrahedra are shaded with crosses, O atoms are large open circles, and hydrogen atoms are small open circles. K–O, Cu–O and O–H bonds are drawn as solid lines.

Cyanochroite: Cyanochroite, $K_2Cu^{2+}(H_2O)_6(SO_4)_2$, has been described from Mount Vesuvius, Italy, where it occurs as a product of volcanic exhalation. It is a Tutton's salt, all of which have the general formula $M^+M^{2+}(H_2O)_6(X^{6+}O_4)_2$. Cyanochroite is a member of the picromerite group, which includes picromerite, $K_2Mg(H_2O)_6(SO_4)_2$, möhrite, $(NH_4)_2Fe(H_2O)_6(SO_4)_2$, boussingaultite, $(NH_4)_2Mg(H_2O)_6(SO_4)_2$ and nickel-boussingaultite, $(NH_4)_2(Ni,Mg)(H_2O)_6(SO_4)_2$. The structure of cyanochroite (Robinson & Kennard 1972) (Fig. 7) contains isolated $Cu^{2+}(H_2O)_6$ octahedra that are weakly bonded to the remainder of the structure by K–O bonds and a network of hydrogen bonds. The Tutton's-salt structure allows considerable flexibility of the geometry of the $M^{2+}(OH_2)_6$ octahedron (Eby & Hawthorne 1993), so that the structure can accommodate a Jahn–Teller distortion of the octahedral environment; thus Cu^{2+} Tutton's salts are strictly isostructural with non-Cu^{2+} Tutton's salts.

Given the structural compliance of the octahedron in the structure of Tutton's salts, it is surprising that the $Cu^{2+}\phi_6$ octahedron in cyanochroite shows the strongest rhombic elongation [(2 + 2 + 2)-distortion] of any mineral, as indicated by the Δ_T parameter (Table 3). If such a compliant arrangement were to accommodate a statically distorted $Cu^{2+}\phi_6$ octahedron, it should show an essentially tetragonal (4 + 2)-distortion geometry. The observed (2 + 2 + 2)-distorted $Cu^{2+}\phi_6$ geometry in cyanochroite is only consistent with a dynamically distorted octahedron, as predicted by Alcock *et al.* (1984) and as reviewed above.

Bayldonite, volborthite and $KCu_3^{2+}(OH)_2[(AsO_4)H(AsO_4)]$: Only two mineral structures contain (2 + 2 + 2)-distorted $Cu^{2+}\phi_6$ octahedra with $\Delta_T > 0.90$ (Table 3). One of these minerals is cyanochroite, in which we have proposed a dynamic Jahn–Teller effect. The other is the $Cu(2)\phi_6$ octahedron in the structure of bayldonite. The Cu–ϕ bond-length distributions in the two minerals with $\Delta_T > 0.90$ are quite similar (Table 3), raising the possibility that the $Cu(2)\phi_6$ octahedron in bayldonite also is dynamically distorted.

As noted above, the structures of bayldonite, volborthite and $KCu_3^{2+}(OH)_2[(AsO_4)H(AsO_4)]$ all contain graphically identical sheets of octahedra and tetrahedra. The (2 + 2 + 2)-distorted $Cu(2)\phi_6$ octahedron in the lower-symmetry sheets in bayldonite is graphically equivalent to the (2 + 4)-distorted $Cu(1)\phi_6$ octahedra in volborthite and $KCu_3^{2+}(OH)_2[(AsO_4)H(AsO_4)]$. We propose that all three of these octahedra are the result of a dynamic Jahn–Teller effect.

Evidence supporting a dynamic Jahn–Teller $Cu^{2+}\phi_6$ octahedron in these structures should be obtainable from the anisotropic-displacement parameters for the octahedral ligands. However, anisotropic-displacement parameters were only reported for two of the oxygen atoms in volborthite. The structure refinement of $KCu_3^{2+}(OH)_2[(AsO_4)H(AsO_4)]$ (Effenberger 1989) is of good quality, and anisotropic-displacement parameters are available. Therefore, the discussion of the anisotropic-displacement parameters that follows is largely in reference to that structure.

$KCu_3^{2+}(OH)_2[(AsO_4)H(AsO_4)]$: The structure of $KCu_3^{2+}(OH)_2[(AsO_4)H(AsO_4)]$ contains two symmetrically distinct $Cu^{2+}\phi_6$ octahedra; one shows a (2 + 4)-distortion [*Cu*(1)], and the other shows a (4 + 2)-distortion [*Cu*(2)]. The *Cu*(1) site has 2/*m* point symmetry such that the four equatorial *Cu*(1)–*O*(3) bonds are equivalent, as are the two apical *Cu*(1)–*OH* bonds (Table 2). The *Cu*(2) site has $\bar{1}$ symmetry, and the octahedron is somewhat (2 + 2 + 2)-distorted (Table 2).

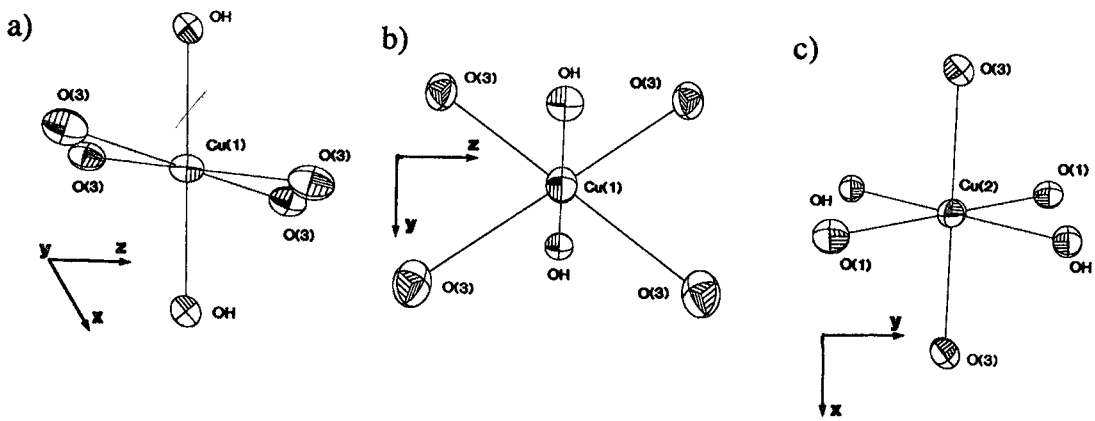

FIG. 8. Anisotropic-displacement ellipsoids for the $Cu^{2+}\phi_6$ octahedra in $KCu_3^{2+}(OH)_2[(AsO_4)H(AsO_4)]$: (a) $Cu(1)\phi_6$; (b) $Cu(1)\phi_6$; (c) $Cu(2)\phi_6$.

Anisotropic-displacement parameters for the $Cu(1)\phi_6$ and $Cu(2)\phi_6$ octahedra are shown in Figure 8. The parameters for the anions of the $Cu(1)\phi_6$ octahedron are consistent with it being dynamically distorted. The maximum principal axis of the O(3) displacement ellipsoid is subparallel to the *Cu*(1)–*O*(3) direction. The *OH* anisotropic-displacement ellipsoid is nearly spherical (Fig. 8), as is normal for a static *M*–ϕ bond. The $Cu(2)\phi_6$ octahedron shows anion anisotropic-displacement parameters consistent with static Jahn–Teller distortion (Fig. 8). In this case, the maximum principal axes of the anions' anisotropic-displacement ellipsoids are not parallel to the *Cu*(2)–ϕ bond directions.

A dynamic $Cu(1)\phi_6$ octahedron must be accommodated by the rest of the structure of $KCu_3^{2+}(OH)_2[(AsO_4)H(AsO_4)]$. Unlike most compounds that show dynamic Jahn–Teller $Cu^{2+}\phi_6$ octahedra, the $Cu(1)\phi_6$ octahedron has strong bonds between the octahedral ligands and other cations in the structure (*i.e.*, Cu^{2+} and As). The environment of the $Cu(1)\phi_6$ octahedron is shown in Figure 9. The *Cu*(1)–*O*(3) bond is dynamic, whereas the *Cu*(1)–*OH* bond is static. Each *O*(3) ligand is also bonded to *Cu*(2) and *As*. The dynamic movement of the *O*(3) ligand of the $Cu(1)\phi_6$ octahedron must result in a distortion of the $Cu(2)\phi_6$ octahedron and a tilting of the AsO_4 tetrahedron. The As cation is bonded to two *O*(3) atoms, an *O*(1) atom and an *O*(2) atom (Fig. 9). The *O*(1) position is a static ligand shared by two *Cu*(2) atoms and acts as an anchor for the AsO_4 tetrahedron. The *O*(2) atom is located at

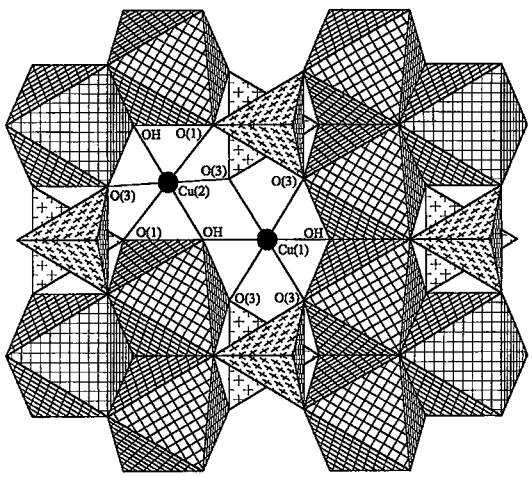

FIG. 9. The detailed environments of the $Cu(1)\phi_6$ and $Cu(2)\phi_6$ octahedra in $KCu_3^{2+}(OH)_2[(AsO_4)H(AsO_4)]$. $Cu^{2+}\phi_6$ octahedra are cross-hatched, and $As\phi_4$ tetrahedra are shaded with crosses.

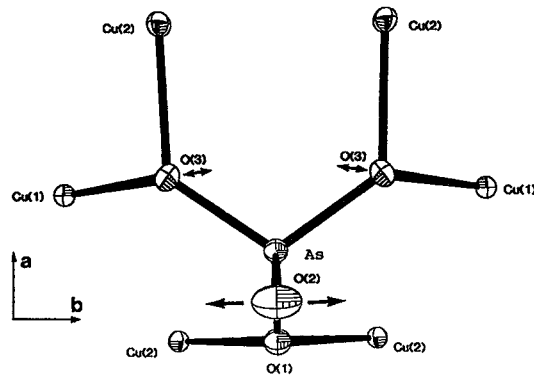

FIG. 10. Anisotropic-displacement ellipsoids for the $As\phi_4$ tetrahedron in the structure of $KCu_3^{2+}(OH)_2[(AsO_4)H(AsO_4)]$.

the AsO_4 apex, and is only very weakly bonded by two long bonds to K (3.24 Å: Effenberger 1989) and by two hydrogen bonds. Tilting of the AsO_4 tetrahedron can easily occur owing to the weak bonding to *O*(2), and may happen in two ways. The coupled motion of both *O*(3) atoms in the same direction will move the *O*(3)–*O*(3) edge of the tetrahedron up and down, such that the *O*(2) apical oxygen will move back and forth along the [100] direction. It is also possible that the two *O*(3) atoms will move out of phase, such that one moves up while the other moves down. In this case, the AsO_4 tetrahedron would rotate about the *As*–*O*(1) bond and the *O*(2) oxygen atom would move back and forth in the [010] direction. Examination of the anisotropic-displacement parameters for the *O*(2) position (Fig. 10) clearly shows significant anisotropic displacement in the [010] direction, indicating that the motion of the two *O*(3) ligands belonging to one AsO_4 tetrahedron are out-of-phase.

Volborthite: The structure of volborthite (Basso *et al.* 1988) contains a $Cu(1)\phi_6$ octahedron analogous to the $Cu(1)\phi_6$ octahedron in $KCu_3^{2+}(OH)_2[(AsO_4)H(AsO_4)]$. However, Basso *et al.* (1988) only gave anisotropic-displacement parameters for two of the oxygen atoms, both of which show anomalously high values. One of these oxygen atoms belongs to the interlayer H_2O group, and the other [*O*(1)] is the apical (non-sheet) oxygen of the VO_4 tetrahedron. In volborthite, this atom of oxygen is shared between two VO_4 tetrahedra that link adjacent sheets, and the V–O–V bond is linear by symmetry constraints. However, Basso *et al.* (1988) argued that the large displacement-parameters associated with the *O*(1) position indicate positional disorder and a nonlinear V–O–V bond. The local environment around the VO_4 tetrahedron is shown in

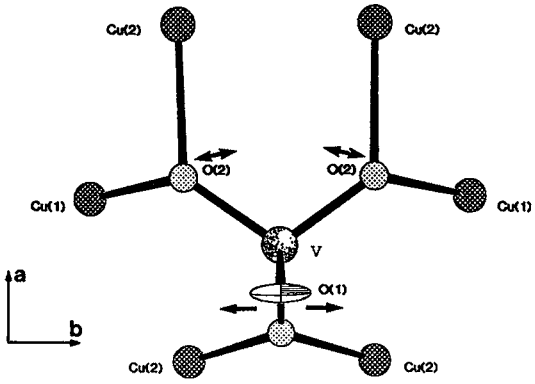

FIG. 11. Anisotropic-displacement ellipsoid for the O(1) site in the structure of volborthite.

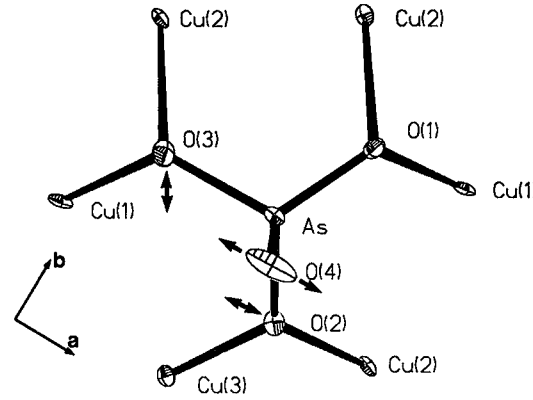

FIG. 12. Anisotropic-displacement ellipsoids for the Asϕ_4 tetrahedron in the structure of bayldonite.

Figure 11. Note that we predict the *Cu*(1)–*O*(2) bonds to be dynamic in this case, as *O*(2) in volborthite is graphically equivalent to *O*(3) in $KCu_3^{2+}(OH)_2[(AsO_4)H(AsO_4)]$. The *O*(1) anisotropic-displacement ellipsoid in volborthite is elongated in the same way as the *O*(2) displacement ellipsoid in $KCu_3^{2+}(OH)_2[(AsO_4)H(AsO_4)]$ (Fig. 11), consistent with a dynamic *Cu*(1)ϕ_6 octahedron, as well as a nonlinear V–O–V bond.

Bayldonite: Arguments based upon the structural relationships between bayldonite, volborthite and $KCu_3^{2+}(OH)_2[(AsO_4)H(AsO_4)]$ (see above) lead to the prediction that the (2 + 2 + 2)-distorted *Cu*(2)ϕ_6 octahedron in bayldonite is dynamically distorted, whereas the *Cu*(1)ϕ_6 and *Cu*(3)ϕ_6 octahedra are statically distorted. The dynamically (2 + 2 + 2)-distorted *Cu*(2)ϕ_6 octahedron is elongated in the *Cu*(2)–*O*(3) direction two-thirds of the time and in the *Cu*(2)–*O*(2) direction one-third of the time. The predicted dynamic interchange of the distortion directions should lead to markedly anisotropic anion-displacement ellipsoids, with their maximum principal axes parallel to the *Cu*–ϕ bonds. The anisotropic-displacement ellipsoids for each $Cu^{2+}\phi_6$ octahedron in bayldonite (Ghose & Wan 1979) are of low precision, owing to the high X-ray absorption (μ_λ = 372 cm^{-1}) and poor quality of the crystal, and some of the ellipsoids apparently show anomalous shapes. However, the anisotropic-displacement parameters are generally consistent with the proposed dynamic $Cu^{2+}\phi_6$ octahedron in bayldonite.

Dynamic distortion of the *Cu*(1)ϕ_6 octahedra in the structures of volborthite and $KCu_3^{2+}(OH)_2[(AsO_4)H(AsO_4)]$ is accommodated by tilting of the tetrahedral group, as shown in Figures 10 and 11. Note that in both cases, the tetrahedrally coordinated cation is located on a mirror plane. The coupled movement of the ligands on either side of the mirror plane causes the apical tetrahedral ligand to sweep out a path perpendicular to the mirror plane, as shown by the anisotropic-displacement ellipsoids (Figs. 10, 11).

The situation is somewhat more complicated in the structure of bayldonite. The local environment of the AsO_4 tetrahedron is shown in Figure 12. The As is located on a general position in the space group *C*2/*c*, and each of the four tetrahedral ligands are symmetrically distinct. Also, the tetrahedron shares its ligands with two pairs of three symmetrically distinct Cu^{2+} ions. Of these, only the *Cu*(2)ϕ_6 octahedron is dynamically distorted. The effect of the dynamic ligands on the tetrahedron is somewhat different from that observed in the volborthite and $KCu_3^{2+}(OH)_2[(AsO_4)H(AsO_4)]$ structures. In this case, the *Cu*(2)–*O*(3) and *Cu*(2)–*O*(2) bonds are dynamic, as indicated by arrows in Figure 12. Also, the *Cu*(2)–*O*(3) bond is elongated two-thirds of the time, whereas the *Cu*(2)–*O*(2) bond is only elongated one-third of the time. For a given AsO_4 tetrahedron, the *Cu*(2)–*O*(3) bond is elongated while the *Cu*(2)–*O*(2) bond is shortened, and the *Cu*(2)–*O*(3) bond is shortened while the *Cu*(2)–*O*(2) bond is elongated. This coupled dynamic movement rotates the tetrahedron such that the apical *O*(4) position rocks back and forth, as clearly shown by the *O*(4) displacement ellipsoid in Figure 12.

DISCUSSION

(1) It is only after careful examination of the geometries of all $Cu^{2+}\phi_6$ octahedra in Cu^{2+} oxysalt minerals that the true importance of the Jahn–Teller effect is apparent. We have shown that probably every $Cu^{2+}\phi_6$ octahedron observed in Cu^{2+} oxysalt minerals is distorted due to the Jahn–Teller effect: *there is no*

conclusive example of a true holosymmetric $Cu^{2+}\phi_6$ octahedron in these minerals.

(2) The (4 + 2)-distorted $Cu^{2+}\phi_6$ octahedral geometry is by far the most common in Cu^{2+} oxysalt minerals and in Cu^{2+} compounds in general. However, a considerable range of Cu–ϕ bond-lengths is observed in these octahedra, with the apical bond-lengths showing the most dispersion. The (4 + 2)-distorted $Cu^{2+}\phi_6$ octahedron is flexible and responds to steric effects of the crystal structure.

(3) It remains unclear whether any (2 + 4)-distorted $Cu^{2+}\phi_6$ octahedra occur in minerals. Possible examples are in the structures of campigliaite, paratacamite, volborthite and demesmaekerite. Of these, those observed in campigliaite are from such an imprecise structure-refinement that the bond lengths cannot be considered reliable. The structure of volborthite contains a (2 + 4)-distorted $Cu^{2+}\phi_6$ octahedron, but strong arguments have been advanced that the octahedron is dynamically distorted, a time average of two unaligned (4 + 2)-distorted octahedra. The paratacamite structure reportedly contains a (2 + 4)-distorted octahedron (Fleet 1975), but the refinement involved a substructure, and as a consequence, anisotropic-displacement parameters were not refined for the octahedron's ligands. This octahedron may also be dynamically distorted. Finally, there is a single (2 + 4)-distorted octahedron in the structure of demesmaekerite. This octahedron is the most persuasive example of a true (2 + 4)-distorted $Cu^{2+}\phi_6$ octahedron, as the anisotropic-displacement ellipsoids reported by Ginderow & Cesbron (1983) do not conclusively indicate that the octahedron is dynamically distorted.

(4) Mineralogists have always assumed that dynamically distorted $Cu^{2+}\phi_6$ octahedra do not occur in minerals. However, it seems probable that dynamically distorted $Cu^{2+}\phi_6$ octahedra do occur in the structures of cyanochroite, volborthite and bayldonite; two of these structures have (2 + 2 + 2)-distorted octahedra. Furthermore, a number of other Cu^{2+} oxysalt minerals also show (2 + 2 + 2)-distorted octahedra (Table 3), and it is possible that some of these may also be dynamically distorted.

Acknowledgements

The Natural Sciences and Engineering Research Council of Canada supported this work with Post-Graduate and Post-Doctoral Fellowships to PCB, and an Operating Grant to FCH. This manuscript was improved following reviews by Dr. M.E. Fleet and an anonymous reviewer, and editorial work by Dr. J.M. Hughes and Dr. R.F. Martin.

References

Alcock, N.W., Duggan, M., Murray, A., Tyagi, S., Hathaway, B.J. & Hewat, A. (1984): The low-temperature crystal structure (203 and 123 K) and electronic properties of diammonium hexa-aquacopper(II) disulphate: a fluxional CuO_6 chromophore. *J. Chem. Soc. Dalton Trans.*, 7-14.

Bacci, M. (1979): Jahn–Teller effect in transition metal ions: a parameterization method based on the angular overlap model. *Chem. Phys.* **40**, 237-244.

Basso, R., Palenzona, A. & Zefiro, L. (1988): Crystal structure refinement of volborthite from Scrava mine (eastern Liguria, Italy). *Neues Jahrb. Mineral. Monatsh.*, 385-394.

———, ——— & ——— (1989): Crystal structure refinement of a Sr-bearing term related to copper vanadates and arsenates of adelite and descloizite groups. *Neues Jahrb. Mineral. Monatsh.*, 300-308.

Bersuker, I.B. (1984): *The Jahn–Teller Effect and Vibronic Interaction in Modern Chemistry.* Plenum Press, New York, N.Y.

Blackburn, A.C., Gallucci, J.C. & Gerkin, R.E. (1991): Structure of hexaaquacopper(II) bromate. *Acta Crystallogr.* **C47**, 2019-2023.

Brown, G.M. & Chidambaram, R. (1969): The structure of copper ammonium sulfate hexahydrate from neutron-diffraction data. *Acta Crystallogr.* **B25**, 676-687.

Brown, I.D. (1981): The bond-valence method: an empirical approach to chemical structure and bonding. *In* Structure and Bonding in Crystals II (M. O'Keeffe & A. Natvrotsky, eds.). Academic Press, New York, N.Y. (1-30).

Burdett, J.K. (1980): *Molecular Shapes: Theoretical Models of Inorganic Stereochemistry.* Wiley, New York, N.Y.

Burns, P.C., Cooper, M.A. & Hawthorne, F.C. (1995): Claringbullite: a Cu^{2+} oxysalt with Cu^{2+} in trigonal-prismatic coordination. *Can. Mineral.* **33**, 633-639.

——— & Hawthorne, F.C. (1995a): Mixed-ligand $Cu^{2+}\phi_6$ octahedra in minerals: observed stereochemistry and Hartree–Fock calculations. *Can. Mineral.* **33**, 1177-1188.

——— & ——— (1995b): Coordination-geometry structural pathways in Cu^{2+} oxysalt minerals. *Can. Mineral.* **33**, 889-905.

Cid-Dresdner, H. (1965): Determination and refinement of the crystal structure of turquoise, $CuAl_6(PO_4)_4(OH)_8{\cdot}4H_2O$. *Z. Kristallogr.* **121**, 87-113.

Cocco, G., Fanfani, L. & Zanazzi, P.F. (1967): The crystal structure of fornacite. *Z. Kristallogr.* **124**, 385-397.

CULLEN, D.L. & LINGAFELTER, E.C. (1971): Redetermination of the crystal structure of potassium lead hexanitrocuprate(II), $K_2PbCu(NO_2)_6$, *Inorg. Chem.* **10**, 1264-1268.

DEETH, R.J. & HITCHMAN, M.A. (1986): Factors influencing Jahn–Teller distortions of six-coordinate copper (II) and low-spin nickel (II) complexes. *Inorg. Chem.* **25**, 1225-1233.

EBY, R.K. (1988): *Copper Oxysalts: The Jahn–Teller Effect and its Structural Implications*. M.Sc. thesis, Univ. of Manitoba, Winnipeg, Manitoba.

_____ & HAWTHORNE, F.C. (1993): Structural relations in copper oxysalt minerals. I. Structural hierarchy. *Acta Crystallogr.* **B49**, 28-56.

EFFENBERGER, H. (1985): $Cu_2O(SO_4)$, dolerophanite: refinement of the crystal structure, with a comparison of $[OCu(II)_4]$ tetrahedra in inorganic compounds. *Monatsh. Chem.* **116**, 927-931.

_____ (1989): An uncommon $Cu^{[2\,+\,4]}O_6$ coordination polyhedron in the crystal structure of $KCu_3(OH)_2[(AsO_4)H(AsO_4)]$ (with a comparison to related structure types). *Z. Kristallogr.* **188**, 43-56.

_____ & PERTLIK, F. (1988): Comparison of the homeomorphic crystal structures of $Pb(Fe,Mn)(VO_4)(OH)$ = čechite and $PbCu(AsO_4)(OH)$ = duftite. *Z. Kristallogr.* **185**, 610.

ENGLMAN, R. (1972): *The Jahn–Teller Effect in Molecules and Crystals*. Wiley-Interscience, London, U.K.

FANFANI, L., NUNZI, A., ZANAZZI, P.F. & ZANZARI, A.R. (1973): The crystal structure of buttgenbachite. *Mineral. Mag.* **39**, 264-270.

_____ & ZANAZZI, P.F. (1968): The crystal structure of vauquelinite and the relationships to fornacite. *Z. Kristallogr.* **126**, 433-443.

FLEET, M.E. (1975): The crystal structure of paratacamite, $Cu_2(OH)_3Cl$. *Acta Crystallogr.* **B31**, 183-187.

GAŽO, J., BERSUKER, I.B., GARAJ, J., KAHEŠOVÁ, M., KOHOUT, J., LANGFELDEROVÁ, H., MELNÍK, M., SERÁTOR, M. & VALACH, F. (1976): Plasticity of the coordination sphere of copper(II) complexes, its manifestation and causes. *Coord. Chem. Rev.* **19**, 253-297.

GHOSE, S. & WAN, CHE'NG (1979): Structural chemistry of copper and zinc minerals. VI. Bayldonite, $(Cu,Zn)_3Pb(AsO_4)_2(OH)_2$: a complex layer structure. *Acta Crystallogr.* **B35**, 819-823.

GINDEROW, D. & CESBRON, F. (1983): Structure de la demesmaekerite, $Pb_2Cu_5(SeO_3)_6(UO_2)_2(OH)_6{\cdot}2H_2O$. *Acta Crystallogr.* **C39**, 824-827.

GIUSEPPETTI, G., MAZZI, F. & TADINI, C. (1989): The crystal structure of chalcosiderite, $CuFe_6^{3+}(PO_4)_4(OH)_8{\cdot}4H_2O$. *Neues Jahrb. Mineral. Monatsh.*, 227-239.

GRICE, J.D., SZYMAŃSKI, J.T. & JAMBOR, J.L. (1996): The crystal structure of clinoatacamite, a new polymorph of $Cu_2(OH)_3Cl$. *Can. Mineral.* **34**, 73-78.

HATHAWAY, B.J. (1984): A new look at the stereochemistry and electronic properties of complexes of the copper(II) ion. *Structure and Bonding* **57**, 55-118.

_____, DUGGAN, M., MURPHY, A., MULLANE, J., POWER, C., WALSH, A. & WALSH, B. (1981): The stereochemistry and electronic properties of fluxional six-coordinate copper(II) complexes. *Coord. Chem. Rev.* **36**, 267-324.

HAWTHORNE, F.C., GROAT, L.A. & EBY, R.K. (1989): Antlerite, $Cu_3SO_4(OH)_4$, a heteropolyhedral wallpaper structure. *Can. Mineral.* **27**, 205-209.

HITCHMAN, M.A., MCDONALD, R.G. & REINEN, D. (1986): EPR spectrum of tetragonally compressed CuF_4^{4-}: ligand and metal hyperfine parameters. *Inorg. Chem.* **25**, 519-522.

HUGHES, J.M., STARKEY, S.J., MALINCONICO, M.L. & MALINCONICO, L.L. (1987): Lyonsite, $Cu_3^{2+}Fe_4^{3+}(VO_4)_6^{3-}$, a new fumarolic sublimate from Izalco volcano, El Salvador: descriptive mineralogy and crystal structure. *Am. Mineral.* **72**, 1000-1005.

JAHN, H.A. & TELLER, E. (1937): Stability of polyatomic molecules in degenerate electronic states. *Proc. Roy. Soc., Ser.* A **161**, 220-235.

JAMBOR, J.L., DUTRIZAC, J.E., ROBERTS, A.C., GRICE, J.D. & SZYMAŃSKI, J.T. (1996): Clinoatacamite, a new polymorph of $Cu_2(OH)_3Cl$, and its relationship to paratacamite and "anarakite". *Can. Mineral.* **34**, 61-72.

KRACHER, A. & PERTLIK, F. (1983): Zinkreicher Paratacamit, $Cu_3Zn(OH)_6Cl_2$, aus der Herminia Mine, Sierra Gorda, Chile. *Ann. Naturhist. Mus. Wien* **85/A**, 93-97.

LIEHR, A.D. & BALLHAUSEN, C.J. (1958): Inherent configurational instability of octahedral inorganic complexes in *Eg* electronic states. *Ann. Phys.* **3**, 304-319.

LOHR, L.L. JR. & LIPSCOMB, W.N. (1963): An LCAO–MO study of static distortions of transition metal complexes. *Inorg. Chem.* **2**, 911-917.

MASSEY, A. (1973): *Comprehensive Inorganic Chemistry*. Oxford Univ. Press, Oxford, U.K.

MCLEAN, W.J. & ANTHONY, J.W. (1972): The disordered, "zeolite-like" structure of connellite. *Am. Mineral.* **57**, 426-438.

MONTGOMERY, H. & LINGAFELTER, E.C. (1966): The crystal structure of Tutton's salts. III. Copper ammonium sulfate hexahydrate. *Acta Crystallogr.* **20**, 659-662.

MULLEN, D., HEGER, G. & REINEN, D. (1975): Planar dynamic Jahn–Teller effects in nitrocomplexes: a single crystal neutron diffraction study of $Cs_2PbCu(NO_2)_6$ at 293 K. *Solid State Commun.* **17**, 1249-1252.

ÖPIK, U. & PRYCE, F.R.S. (1957): Studies of the Jahn–Teller effect. I. A survey of the static problem. *Proc. Roy. Soc. London, Ser.* **A 238**, 425-447.

ORGEL, L.E. (1966): *An Introduction to Transition Metal Chemistry: Ligand-Field Theory* (second ed.). Methuen, London, U.K.

QURASHI, M.M. & BARNES, W.H. (1963): The structures of the minerals of the descloizite and adelite groups. IV. Descloizite and conichalcite. Part 2. The structure of conichalcite. *Can. Mineral.* **7**, 561-577.

REINEN, D. & KRAUSE, S. (1981): Local and cooperative Jahn–Teller interactions of copper(2+) in host lattices with tetragonally compressed octahedra. Spectroscopic and structural investigations of the mixed crystals $K(Rb)_2Zn_{1-x}Cu_xF_4$. *Inorg. Chem.* **20**, 2750-2759.

ROBINSON, D.C. & KENNARD, C.H.L. (1972): Potassium hexa-aquacopper(II) sulfate, $CuH_{12}K_2O_{14}S_2$ (neutron). *Cryst. Struct. Commun.* **1**, 185-188.

SABELLI, C. (1982): Campigliaite, $Cu_4Mn(SO_4)_2(OH)_6{\cdot}4H_2O$, a new mineral from Campiglia Marihima, Tuscany, Italy. II. Crystal structure. *Am. Mineral.* **67**, 388-393.

_____ & ZANAZZI, P.F. (1972): The crystal structure of devillite. *Acta Crystallogr.* **B28**, 1182-1189.

SHANNON, R.D. (1976): Revised effective ionic radii and systematic studies of interatomic distances in halides and chalcogenides. *Acta Crystallogr.* **A32**, 751-767.

SHIELDS, K.G. & KENNARD, C.H.L. (1972): Caesium hexa-aquacopper(II) sulfate, $Cs_2CuH_{12}O_{14}S_2$ (neutron). *Cryst. Struct. Commun.* **1**, 189-191.

_____, VAN DER ZEE, J.J. & KENNARD, C.H.L. (1972): Thallium hexaaquacopper(II) sulfate, $CuH_{12}O_{14}S_2Tl_2$ (neutron). *Cryst. Struct. Commun.* **1**, 371-373.

SHOEMAKER, G.L., ANDERSON, J.B. & KOSTINER, E. (1977): Refinement of the crystal structure of pseudomalachite. *Am. Mineral.* **62**, 1042-1048.

_____, _____ & _____ (1981): The crystal structure of a third polymorph of $Cu_5(PO_4)_2(OH)_4$. *Am. Mineral.* **66**, 169-175.

SIDGWICK, N.V. (1950): *The Chemical Elements and Their Compounds.* Clarenden Press, Oxford, U.K.(??sp)

SIEBER, N., HOFMEISTER, W., TILLMANNS, E. & ABRAHAM, K. (1984): Neue Mineraldaten für Kupferphosphate und-Arsenate von Reichenbach. *Fortschr. Mineral.* **62**, 231-233.

SMITH, G., MOORE, F.H. & KENNARD, C.H.L. (1975): Rubidium hexaaquacopper (II) sulphate, $CuH_{12}O_{14}Rb_2S_2$ (neutron – low temperature). *Cryst. Struct. Commun.* **4**, 407-412.

VAN DER ZEE, J.J., SHIELDS, K.G., GRAHAM, A.J. & KENNARD, C.H.L. (1972): Rubidium hexa-aquacopper(II) sulfate, $CuH_{12}O_{14}Rb_2S_2$. *Cryst. Struct. Commun.* **1**, 367-369.

VARAKSINA, T.V., FUNDAMENSKY, V.S., FILATOV, S.K. & VERGASOVA, L.P. (1990): The crystal structure of kamchatkite, a new naturally occuring oxychloride sulphate of potassium and copper. *Mineral. Mag.* **54**, 613-616.

WEBB, M.W., KAY, H.F. & GRIMES, N.W. (1965): The structure of ammonium copper sulphate $(NH_4)_2Cu(SO_4)_2{\cdot}6H_2O$. *Acta Crystallogr.* **18**, 740-742.

WILDNER, M. & GIESTER, G. (1988): Crystal structure refinements of synthetic chalcocyanite ($CuSO_4$) and zincosite ($ZnSO_4$). *Mineral. Petrol.* **39**, 201-209.

YAMATERA, H. (1979): Jahn–Teller distortion in copper(II) complexes. Why tetragonal elongation is preferred to tetragonal compression. *Acta Chem. Scand.* **A33**, 107-111.

ZIGAN, F., JOSWIG, W., SCHUSTER, H.D. & MASON, S.A. (1977): Verfeinerung der Struktur von Malachit, $Cu_2(OH)_2CO_3$, durch Neutronenbeugung. *Z. Kristallogr.* **145**, 412-426.

Received March 8, 1996, revised manuscript accepted July 27, 1996.